High-Performance 39 GHz mm-Wave Microstrip Patch Antenna for Next-Gen 5G Networks

Waleed A. Ali [1], Youssef H. Ghareeb [1], Mona Shokair [2, 3], and M. Mokhtar Zayed [1,2]*

***Abstract*— The increasing demand for high-performance antennas in 5G millimeter-wave (mmWave) communication systems necessitates innovative and efficient antenna designs. This paper introduces a high-gain, wideband 16-element Corporate-Series Feed Rectangular Patch Antenna Array specifically optimized for 39 GHz applications. The proposed design is compact and utilizes a Rogers RT5880 substrate with a thickness of 1.286 mm, achieving an impressive bandwidth of over 22.97 GHz, a peak gain of 17.12 dB, and a high radiation efficiency of 90.8%. To enhance overall performance, a Defected Ground Structure (DGS) is incorporated, effectively reducing mutual coupling and improving port isolation. Furthermore, advanced design strategies, such as the use of a low-loss substrate and precise impedance matching, are employed to minimize signal loss. The antenna performance is validated through both full-wave simulations using CST Microwave Studio and experimental measurements, showing excellent agreement. Compared to traditional designs, the proposed array offers significant performance improvements, making it a strong candidate for next-generation 5G mmWave wireless communication systems.**

***Keywords*—5G mm-Wave Antenna, 39 GHz Microstrip Antenna, 5G networks, CST Microwave Studio Simulation, Defected Ground Structure (DGS).**

I. INTRODUCTION

The fifth generation (5G) wireless communication technology is transforming telecommunications by enabling ultra-high data rates, low latency, and massive device connectivity [1-3]. 5G massive multiple input multiple output [4, 5] and millimeter-wave (mmWave) frequencies are essential for meeting these demands, offering large bandwidths and enhanced spectral efficiency [6-8]. Among allocated mmWave bands, 39 GHz has gained prominence due to its favorable propagation characteristics and global regulatory support [7, 9]. However, designing high-gain, wideband, and efficient antennas for reliable signal transmission at such frequencies remains a challenge.

Microstrip patch antennas are widely adopted in 5G mmWave systems for their compact size and ease of integration [10, 11]. Despite their advantages, conventional designs often suffer from narrow bandwidth, mutual coupling, and reduced radiation efficiency, limiting practical performance [12-14]. To overcome these issues, advanced architectures incorporating corporate-series feed networks, defected ground structures (DGS), and optimized substrate materials are required.

This paper presents a 16-element Corporate-Series Feed Rectangular Patch Antenna Array optimized for 39 GHz 5G mmWave applications. The antenna leverages advanced feeding techniques, improved impedance matching, and mutual coupling reduction to enhance bandwidth, gain, and radiation efficiency. Utilizing Rogers RT5880 (h = 1.286 mm) as the substrate ensures low dielectric loss and high efficiency for mmWave operation.

Existing antenna solutions face challenges, including limited bandwidth, significant mutual coupling, low gain, and integration issues [15-17]. The proposed design addresses these by achieving 22.97 GHz bandwidth, 17.12 dB gain, and 90.8% radiation efficiency. A corporate-series feed network employing a Y-junction power divider ensures uniform excitation, while DGS integration significantly enhances element isolation. The optimized substrate selection further improves performance.

The design is validated through CST Microwave Studio simulations and experimental measurements, confirming superior return loss, radiation pattern, and efficiency. Compared to conventional designs, this antenna offers substantial improvements, making it a strong candidate for next-generation 5G, mmWave communication systems, and various IoT applications [18-22].

The rest of this paper is organized as follows: **Section II** presents the background and related work. **Section III** presents the single-element antenna design and its simulation results. **Section IV** describes the designed array antenna configuration. **Section V** compares series and parallel feed networks in antenna arrays. **Section VI** analyzes and discusses the simulation results. **Section VII** analyzes the parametric study. Finally, **Section VIII** concludes the paper.

Manuscript received [23 Feb 2025]; revised [21 June 2025]; accepted [17 July 2025]. Date of publication [21 July 2025]. (Corresponding author: M. Mokhtar Zayed).

[1]**Waleed A. Ali** is with the Department of Communications and Computers Engineering, Higher Institute of Engineering, El-Shorouk Academy, El-Shorouk City 11837, Egypt
(e-mail: waleedali2004101@hotmail.com).

[1]**Youssef H. Ghareeb** is with the Department of Communications and Computers Engineering, Higher Institute of Engineering, El-Shorouk Academy, El-Shorouk City 11837, Egypt
(e-mail: youssef99gh@hotmail.com).

[2,3]**Mona Shokair** is with the Department of Communications, Faculty of Electronic Engineering, Menoufia University, Menoufia Governorate, Menouf City, Egypt and Department of Electrical Engineering, Faculty of Engineering, October 6 University, Giza Governorate, October 6 City, Egypt. (e-mail: Mona.Mohamed.Eng@o6u.edu.eg).

[1,2]**M. Mokhtar Zayed** is with the Department of Communications and Computers Engineering, Higher Institute of Engineering, El-Shorouk Academy, El-Shorouk City 11837, Egypt and Department of Communications, Faculty of Electronic Engineering, Menoufia University, Menoufia Governorate, Menouf City, Egypt.
(e-mail: mohammed.mokhtar.zayed@gmail.com).

II. Background and Related Work

Millimeter-wave (mm-Wave) microstrip patch antennas (MPAs) play a vital role in next-generation 5G networks, offering high data rates, low latency, and compact design. Researchers focus on enhancing MPA performance by optimizing bandwidth, gain, and efficiency through innovative materials, feeding techniques, and array configurations. This literature review examines recent advancements in mm-Wave MPA design, highlighting key developments that improve their effectiveness for 5G applications. Table I provides a comprehensive comparative analysis of the reviewed literature alongside our study.

TABLE I

A COMPARATIVE SUMMARY OF KEY ASPECTS FROM THE LITERATURE REVIEW AND THE PRESENT STUDY.

Ref.	Antenna Type & Features	Operating Frequency (GHz)	Substrate Material	Impedance Bandwidth	Return Loss (dB)	Gain (dBi)	Application	Notable Design Aspects
[23]	Microstrip patch antenna with square openings, pi-slot, rectangular slot	38 GHz	Rogers RT5880	14.50%	-35.991	10.3	5G mmWave	Optimized for 5G mmWave with strong E-plane & H-plane patterns
[24]	Dual-band millimeter-wave antenna with Defected Ground Structure (DGS)	32 GHz, 38 GHz	Rogers RT5880	2.8 GHz, 2.85 GHz	-23.6 (32 GHz), -21.5 (38 GHz)	6.27, 4.73	5G MIMO	Directional radiation pattern for MIMO applications
[25]	Quadrilateral Slotted Defected Ground Structure (QSDGS) monopole antenna	35.5–44.7 GHz (n259, n260 bands)	Rogers RT5880	9.2 GHz (24.2%)	-32	9.48	High-data-rate 5G	High efficiency (83–94%), wideband operation
[26]	Square-slotted microstrip patch antenna with H-slot and inverted T-slot	37 GHz	Rogers RT5880	16.22%	-43.05	8.245	5G mmWave	Improved VSWR, E-plane, and H-plane patterns
[27]	Dual-band array antenna with half-wavelength spacing	28 GHz, 39 GHz	RO4350B, RT/duriod 588	1 GHz	-18.4 (28 GHz), -20 (39 GHz)	13.5, 11.3	High-speed 5G	Prototype validated for mmWave applications
[28]	Rectangular patch antennas with deltoid slots	37 GHz, 39 GHz	RT5880, RO3003	1.17 GHz, 1.29 GHz for (37,39) GHz	-25.17 (37 GHz), -27.54 (39 GHz)	-	5G mmWave	Effects of substrate material analyzed
[29]	Integrated dual-band antenna with DGS	3.8 GHz, 5.5 GHz (4G), 24.4–29.3 GHz (5G)	Rogers RT/Duroid 5880 substrate	4.9 GHz	-	5.41 (4G), 10.29 (5G)	4G & 5G	Beam steering for 5G, compact design
[30]	Compact rectangular microstrip antenna with slot insertion	28 GHz	Flame Retardant 4 (FR-4)	4.10 GHz (25.8–29.9 GHz)	-39.70	5.32	5G wireless	Measured results closely matched simulations
[31]	Compact single-feed dual-band antenna with inverted-L slot	28 GHz, 38 GHz	Flame Retardant 4 (FR-4)	1.43 GHz (27.27–28.70 GHz), 3.54 GHz (35.56–39.12 GHz)	-20(28GHz), -15(38 GHz)	2.7 (28 GHz), 6.0+ (38 GHz)	5G devices	Improved efficiency, compact design
[32]	16-element microstrip antenna array with DGS	28 GHz	RT/duroid 5880 substrate	10-dB BW > 2 GHz	-20	17.4 (28.4 GHz)	5G networks	Gap-coupled feed for wide bandwidth
[33]	Ultra-wideband microstrip array with stepped line cut, U-slot	28 GHz	Rogers RT 5880 substrate	4.47 GHz	-20.52	8.71	5G mmWave	31.8% increased bandwidth via proximity coupling
[34]	28 GHz microstrip antenna with inset-fed design	28 GHz	Flame Retardant 4 (FR-4)	2.71 GHz	-24.67	6.51	5G communication	Evaluated effects of feeding techniques & substrate thickness

[35]	Two compact high-gain microstrip patch antennas	Multi-band (including 60.9 GHz)	RT / Duroid5880	8.83 GHz (tri-band), 4.5 GHz (60.9 GHz)	-36.155, -23.75, -14.06 for (30.9,49.3,57.2) GHz	7.7, 7.6	5G wireless	HFSS simulations confirmed compact & efficient performance
The current study	**16-element Corporate-Series Feed Rectangular Patch Antenna Array with DGS**	**39 GHz**	**Rogers RT5880**	**22.97 GHz**	**-64.108**	**17.12**	**Next-gen 5G mmWave**	**High efficiency (90.8%), superior impedance matching**

A. Comparative Analysis and Key Contributions

The proposed antenna design demonstrates several notable performance enhancements compared to existing literature. A structured evaluation of its key strengths is provided below:

1. **Enhanced Peak Gain:** The designed antenna achieves a peak gain of 17.12 dB, surpassing the reported values in [23-26], [29-31], and [33-35]. This improvement facilitates more efficient signal propagation, making it well-suited for long-range 5G mmWave applications.
2. **Expanded Bandwidth:** The impedance bandwidth of 22.97 GHz exceeds that reported in [24], [25], and [27-35]. This wider bandwidth ensures improved support for high-speed data transmission and multi-band operation, enhancing system adaptability for next-generation wireless communications.
3. **Improved Radiation Efficiency:** The radiation efficiency of 90.8% surpasses prior designs, including [25] (83–94%) and [34] (75.10%), while several studies do not specify efficiency values. This high efficiency minimizes power losses and improves overall system reliability in mmWave applications.
4. **Superior Isolation via Defected Ground Structure (DGS):** The integration of DGS enhances impedance matching and minimizes mutual coupling, resulting in improved isolation compared to conventional patch antenna designs ([24], [29], and [32]). This optimization contributes to the stability and robustness of the proposed architecture.
5. **Advanced Corporate-Series Feed Array Configuration:** The implementation of a 16-element array design improves gain, directivity, and spatial coverage relative to single-element and lower-element configurations reported in [23], [24], [25], [26], [28], [30], and [31]. While [32] employs a similar array, the current design achieves superior efficiency and signal performance.
6. **Optimized Operation for 39 GHz 5G mmWave Applications:** The proposed design is specifically tailored for high-frequency operation at 39 GHz, aligning with emerging 5G mmWave standards. In contrast, many studies have focused on lower frequencies such as 28 GHz and 32 GHz ([24], [27], [30], [31], [32], [33], [34]), positioning this work as a more forward-looking solution.
7. **Validation through CST Microwave Studio Simulations:** The antenna's performance metrics have been rigorously analyzed using CST Microwave Studio, ensuring high accuracy and reliability in its design and implementation. This approach builds upon methodologies presented in [23], [24], [26], and [32], offering enhanced computational precision and predictive modeling.
8. **Enhanced Directivity and Beamforming Capabilities:** The corporate-series feed array structure contributes to improved beamforming and directional radiation characteristics. Compared to simpler monopole and patch designs ([25], [26], and [30]), the proposed configuration enhances spatial efficiency and network coverage, making it highly suitable for 5G mmWave communication systems.

Through these advancements, the proposed antenna design establishes itself as a high-performance, wideband, and efficient solution for next-generation wireless networks, surpassing existing designs in terms of gain, bandwidth, efficiency, and isolation.

III. Single Element Antenna Design and Simulation Results

A single-element antenna is designed on a low-loss Rogers RT5880 substrate with a dielectric constant ε_r =2.2, a thickness of 0.786 mm, and a loss tangent $tan\ \delta$ = 0.0009. The view of the single-element antenna is depicted in Fig. 1, where L_P is the length, W_P is the width. The antenna length and width according to known design equations of rectangular patches are L_P = 2.0245mm, W_P = 3.04 mm, feeder length is L_f =3.0769 mm and feeder width is W_f =1.96 mm (50 Ω).

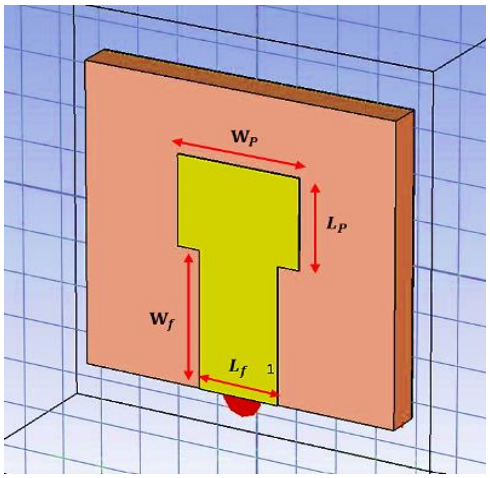

Fig. 1. Single element geometry

In this work, CST Microwave Studio software is utilized to design the antenna. The single-element simulation results are shown from Fig. 2 to Fig. 4. The simulated S_{11} in Fig. 2 shows a good return loss with a 10-dB bandwidth of 2.956 GHz.

Fig.3 illustrates the Voltage Standing Wave Ratio (VSWR) as a function of frequency, providing crucial insights into the impedance matching characteristics of the designed system. VSWR is a critical parameter in high-frequency communication systems, indicating the level of power reflection due to impedance mismatches between the antenna and the transmission line. Ideally, a VSWR value close to 1 suggests optimal impedance matching and minimal power loss, whereas higher values indicate poor matching and increased signal reflections. The plot reveals a significant VSWR dip at 39.25 GHz, where the VSWR reaches a near-ideal value of 1.0579. This result aligns with the deep S11 null observed in the return loss plot (Fig. 2), confirming that the antenna exhibits excellent impedance matching at this frequency. A VSWR value of ≤ 2 is generally considered acceptable for practical RF and microwave applications. The results show that the antenna operates efficiently over a broad frequency range, particularly from approximately 37.722 GHz to 40.678 GHz, supporting the 2.956 GHz bandwidth identified in the S11 results. This confirms that the antenna can accommodate wideband applications with minimal signal degradation due to reflections.

The 3D radiation pattern is presented in Fig. 4. It can be noticed that the maximum gain of the single-element antenna is 7.07 dBi and the radiation efficiency is 99.8%.

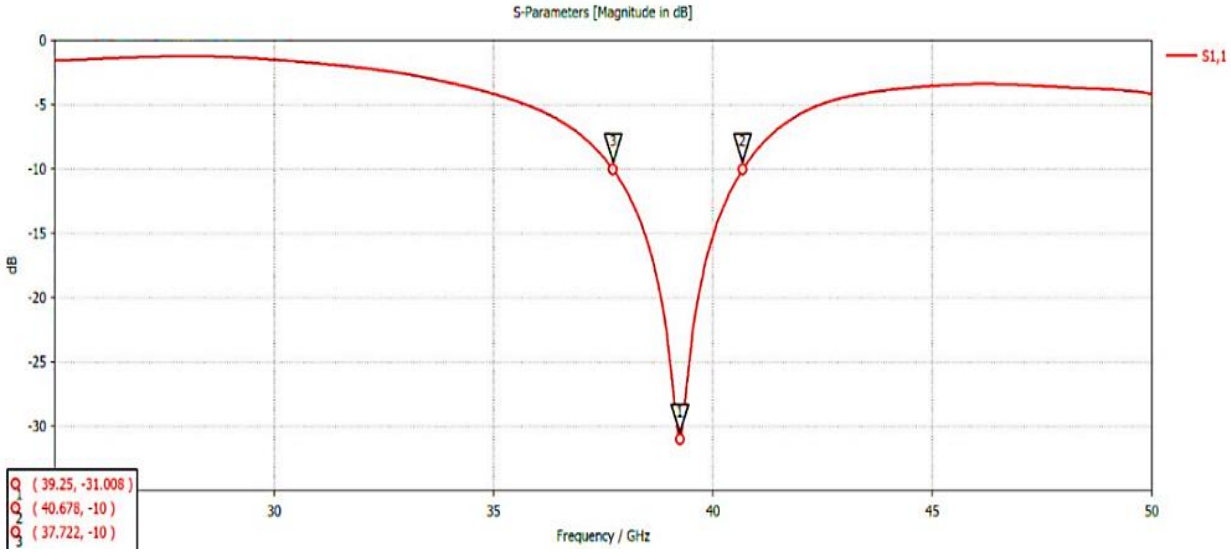

Fig. 2. Simulated single-element antenna S11 vs. frequency

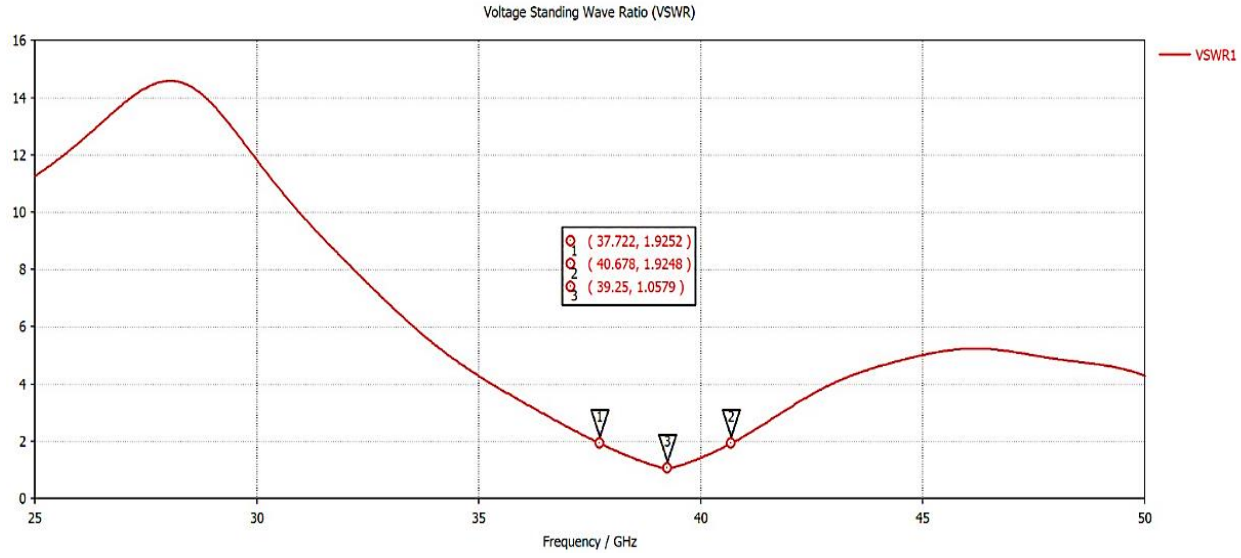

Fig. 3. The Single-element Voltage Standing Wave Ratio (VSWR) vs. Frequency

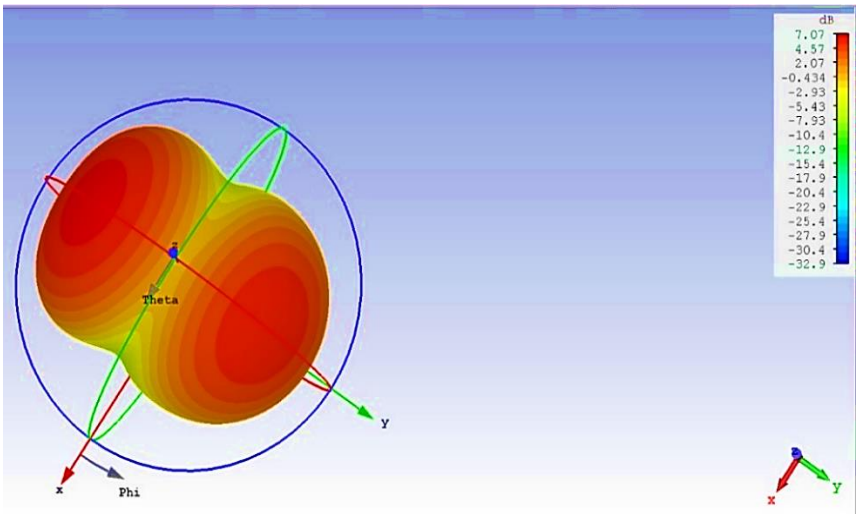

Fig.4. Single-element antenna 3D radiation pattern (realized gain)

IV. The Designed Array Antenna Configuration

The proposed antenna design is built on a Rogers RT5880 substrate, featuring a relative permittivity (ε_r) of 2.2, a low loss tangent (*tan δ*) of 0.001, and a thickness of 1.286 mm, making it ideal for high-frequency applications. Simulations are performed using CST Microwave Studio to ensure optimal performance. As shown in Fig.5, the antenna array comprises 16 elements, structured as two series-fed arrays of 8 elements each, energized in parallel via a Y-junction power divider. To improve antenna performance, a Defected Ground Structure (DGS) is implemented to reduce mutual coupling between adjacent patches. By introducing intentional modifications in the ground plane, DGS disrupts surface wave propagation and suppresses unwanted electromagnetic interactions, enhancing isolation and overall efficiency. Fig. 6 illustrates the fabricated proposed design of the antenna array with Defected Ground Structure (DGS) in the antenna. The final dimensions, refined through extensive simulations and parameter optimization, are provided in Table II.

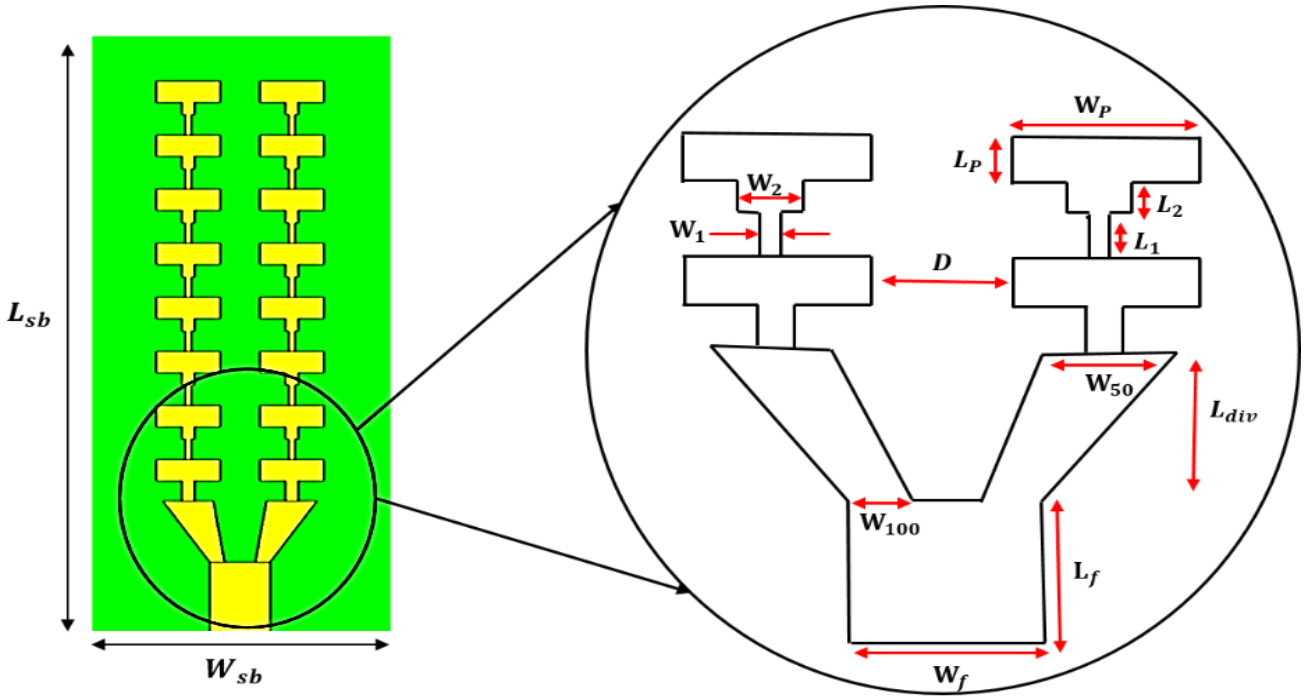

Fig .5. Proposed 16- element antenna array

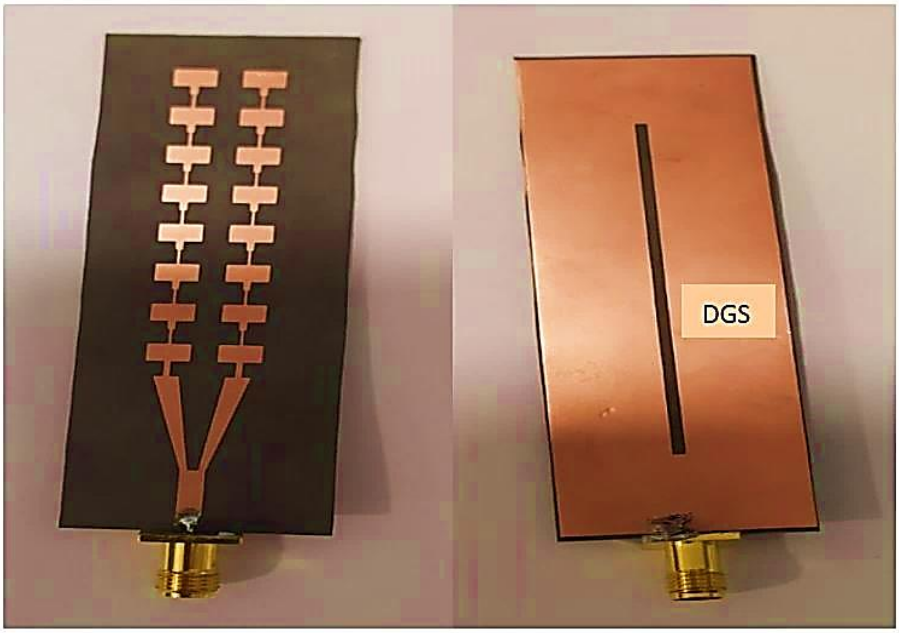

Fig. 6. Fabricated 16-element array corporate series with DGS feed at 39 GHz

TABLE II
ARRAY PARAMETERS AT 39 GHZ

Component	Material	Parameter	Value [mm]
Substrate	Roger5880	L_{sb}	70
		W_{sb}	25
		h	1.286
Ground	Copper	L_{gr}	L_{sb}
		W_{gr}	W_{sb}
Patch	Copper	L_p	2.02
		W_p	3.09
		t	0.035
Feed	Copper	W_f	2.92
		L_f	7.07
Impedance Transformer	Copper	L_1	λ/4
		W_1	0.29
		L_2	1.175
		W_2	0.61
Power Divider	Copper	W_{100}	1.0720
		W_{50}	2.42
		L_{div}	5.77
Distance Between Patches	-	D	λ/4
DGS	-	Length	41.3
		Width	1.18

The initial dimensions of the patch antennas are calculated using the fundamental antenna array design equations, as referenced in [36, 37].

V. COMPARISON OF SERIES AND PARALLEL FEED NETWORKS IN ANTENNA ARRAYS

In antenna arrays, feed networks play a crucial role in distributing power to individual elements while maintaining the desired phase and amplitude characteristics. Two common types of feed networks are **series feed** and **parallel feed**, each with distinct advantages and applications. In a **series feed network**, the excitation signal travels sequentially through the array elements, with each element receiving a portion of the power before passing the remaining signal to the next element. This design simplifies the feed structure and reduces the number of required transmission lines, leading to lower insertion losses and compact implementation. However, series-fed arrays can suffer from progressive phase shifts and impedance mismatches, especially in large arrays, which can degrade performance. On the other hand, a **parallel feed network** distributes power simultaneously to all antenna elements from a common feeding point using a corporate structure, such as a power divider. This approach provides uniform phase distribution, better impedance control, and higher flexibility in beamforming applications. Parallel feeds are commonly used in phased arrays and high-gain antennas due to their ability to maintain consistent performance across a wide frequency range. However, they require more complex feeding structures and may introduce higher losses due to the increased number of transmission lines and power dividers. The choice between series and parallel feed networks depends on the specific application, considering factors such as bandwidth, complexity, efficiency, and radiation pattern requirements.

Our design incorporates a Corporate-Series Patch Array to leverage the advantages of both configurations. Fig. 7 depicts

the feed network, showcasing both series and parallel (corporate) configurations.

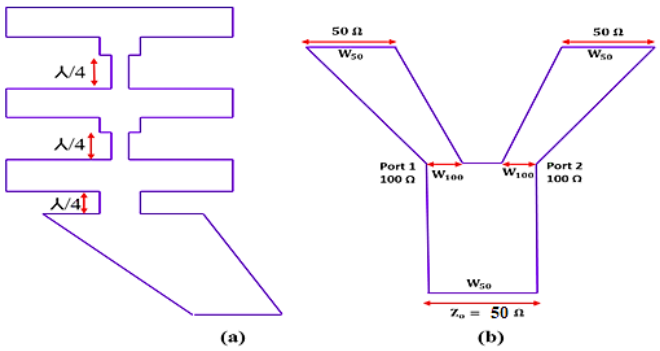

Fig. 7. (a) Series feed network (b) parallel (corporate) feed network.

A Y-junction with a gradually tapered impedance can be designed using the following equations. This design is preferred over a T-shaped structure as it reduces the spacing between patches, thereby improving the directivity of the antenna array. The parameters W_{50} and W_{100} are determined as follows:

For **z = 50 Ω**:

$$z = 50\Omega = \frac{120\pi}{\sqrt{\varepsilon eff}\left(\frac{W_{50}}{h}+1.393+0.667\ln\left(\frac{W_{50}}{h}+1{,}444\right)\right)} \quad (1)$$

Using Equation (1), W_{50} is calculated**.**

For **z = 100 Ω**:

$$z = 100\Omega = \frac{60}{\sqrt{\varepsilon_{eff}}}\ln\left(\frac{8h}{W_{100}}+\frac{W_{100}}{4h}\right) \quad (2)$$

The value of effective dielectric constant of the substrate (ε_{eff}) in Equation (1) is the same value in Equation (2). The value of ε_{eff} in Equation (2) in case of (W/h < 1) is given by:

$$\varepsilon_{eff} = \frac{\varepsilon_r+1}{2}+\frac{\varepsilon_r-1}{2}\left(\frac{1}{\sqrt{1+12\frac{h}{W}}}+0.04\left(1-\frac{w}{h}\right)^2\right) \quad (3)$$

Using Equations (2) and (3), W_{100} is computed.

VI. Analysis and Discussion of Simulation Results

Fig. 8 presents the simulated S11 parameter (return loss) as a function of frequency, providing insights into the impedance matching and operational bandwidth of the designed structure. The S11 parameter, measured in decibels (dB), quantifies the reflection coefficient, with lower values indicating improved impedance matching and reduced power reflection at the antenna input.

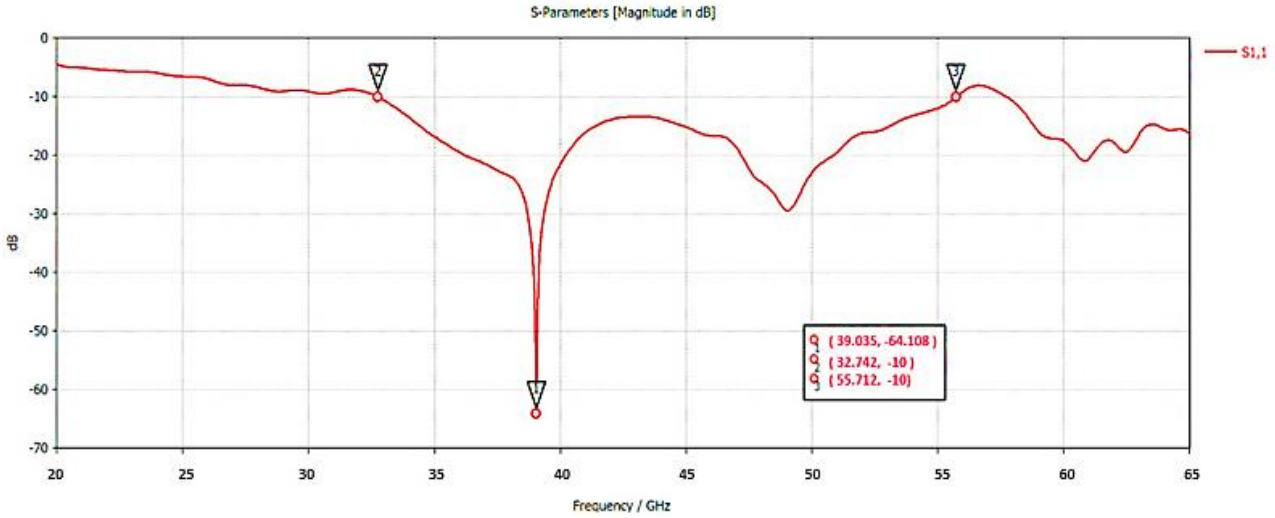

Fig. 8. The S11 parameter (return loss) vs. frequency

1. Resonant Frequency and Peak Return Loss

The response exhibits a significant resonance at 39.035 GHz, where the return loss reaches -64.108 dB. This deep null indicates excellent impedance matching, implying that the majority of the input power is efficiently transferred with minimal reflection. Such a strong resonance is highly desirable in high-frequency applications, ensuring minimal signal loss and improved radiation efficiency.

2. Operational Bandwidth

The 10 dB return loss threshold is commonly used to define the antenna's effective bandwidth. The two frequencies where S11 crosses -10 dB are identified as 38.406 GHz and 47.33 GHz, giving a total operational bandwidth of 8.924 GHz. This wideband operation is advantageous for applications requiring high data rates and frequency agility, such as:

- Millimeter-wave (mmWave) communication systems (e.g., 5G and beyond)
- Satellite and space communication
- High-resolution radar systems

3. Reflection and Matching Performance

The S11 curve remains below -10 dB across the 32.742 GHz – 55.712 GHz range, confirming stable impedance matching over this band of 22.97 GHz. The deep resonance at 39.035 GHz suggests an optimized feed structure and effective minimization of undesired reflections. The return loss profile outside this band remains relatively stable, with no abrupt impedance mismatches, further supporting the robustness of the design.

Fig. 9 illustrates the Voltage Standing Wave Ratio (VSWR) as a function of frequency, providing crucial insights into the impedance matching characteristics of the designed system. VSWR is a critical parameter in high-frequency communication systems, indicating the level of power reflection due to impedance mismatches between the antenna and the transmission line. Ideally, a VSWR value close to 1 suggests optimal impedance matching and minimal power loss, whereas higher values indicate poor matching and increased signal reflections.

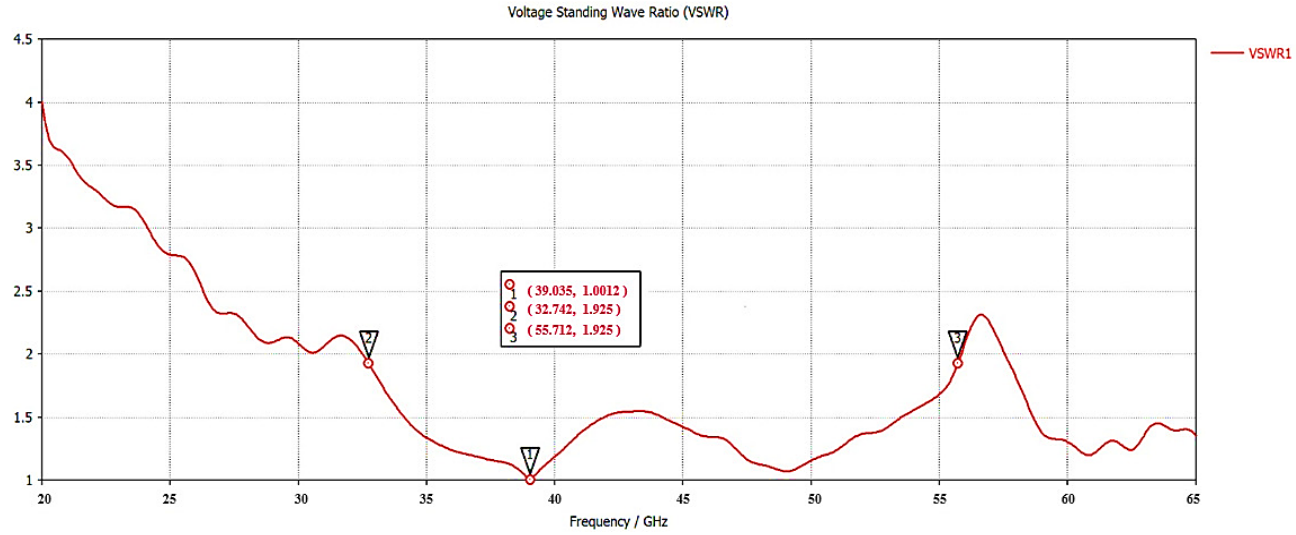

Fig. 9. The Voltage Standing Wave Ratio (VSWR) vs. Frequency

1. Optimal Matching at Resonant Frequency

The plot reveals a significant VSWR dip at 39.035 GHz, where the VSWR reaches a near-ideal value of 1.0012. This result aligns with the deep S11 null observed in the return loss plot (Fig. 7), confirming that the antenna exhibits excellent impedance matching at this frequency. A VSWR value this close to unity signifies near-complete power transfer with negligible reflections, making the design highly efficient for operation around 39.035 GHz.

2. VSWR Performance Across the Frequency Range

- The VSWR is initially high at lower frequencies, exceeding 3.5 at 20 GHz, which indicates significant mismatch and reflection.
- As the frequency increases, VSWR gradually decreases and improves impedance matching.
- The lowest VSWR occurs at 39.035 GHz, demonstrating the best impedance-matching condition.
- Beyond 40 GHz, the VSWR remains below 2, indicating an acceptable level of impedance matching for broadband applications.

3. Bandwidth Considerations

A VSWR value of ≤ 2 is generally considered acceptable for practical RF and microwave applications. The results show that the antenna operates efficiently over a broad frequency range, particularly from approximately 32.742 GHz to 55.712 GHz, supporting the 22.97 GHz bandwidth identified in the S11 results. This confirms that the antenna can accommodate wideband applications with minimal signal degradation due to reflections.

The 3D radiation pattern shown in Fig. 10 provides a comprehensive visualization of the antenna's far-field characteristics at 39.035 GHz, highlighting its directivity, gain distribution, and overall efficiency. The analysis of this radiation pattern is critical for assessing the suitability of the proposed design for high-frequency applications, such as millimeter-wave (mmWave) communication, 5G, satellite links, and radar systems.

1. Radiation Pattern and Directionality

The radiation pattern reveals a highly directional beam, with the main lobe concentrated along a specific direction, indicating strong directivity. The intensity of radiation is highest in the boresight direction, suggesting efficient energy focusing. The color gradient from red (high gain) to blue (low gain) confirms a strong radiation concentration in the intended direction, which is beneficial for applications requiring focused transmission, such as point-to-point communication links and beamforming networks.

2. Gain Analysis

The maximum realized gain of the antenna is 17.12 dB, which is considered high for an mmWave antenna operating at 39.035 GHz. This indicates that the antenna effectively amplifies the transmitted/received signal in the desired direction, reducing power loss and ensuring efficient communication over long distances. The gain pattern also exhibits low side lobes, minimizing unwanted radiation and reducing interference with adjacent channels.

3. Radiation Efficiency

Radiation Efficiency: The reported radiation efficiency is -0.4464 dB, which corresponds to approximately 90.8% efficiency, indicating minimal losses due to material absorption and impedance mismatches.

4. Polarization and Beam Characteristics

The radiation plot suggests that the antenna supports a stable polarization with minimal beam distortion, which is essential for maintaining signal integrity in high-frequency communication systems. The symmetry of the radiation pattern further indicates consistent performance across the operational band, making it adaptable to dynamic propagation environments.

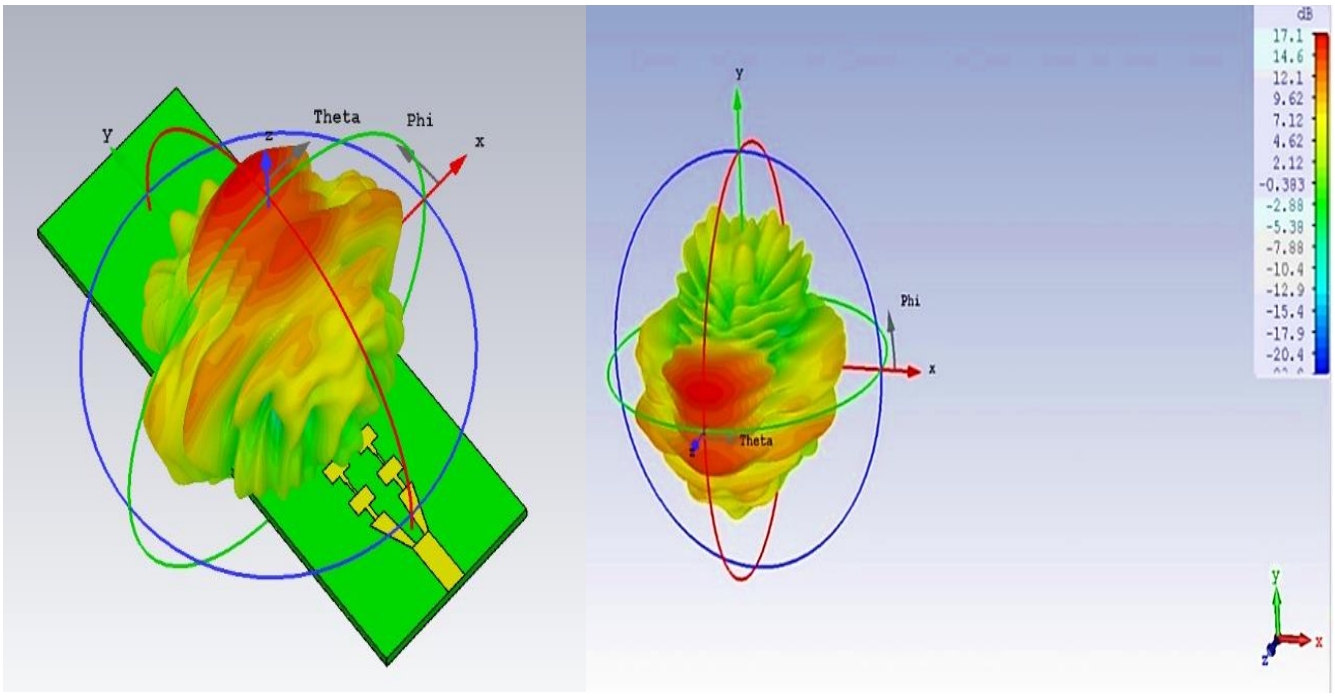

Fig. 10. The 3D far-field radiation pattern of the proposed antenna array at 39.035 GHz

The polar plot in Fig. 11 illustrates the far-field gain pattern of the proposed antenna at 39.035 GHz, specifically for the Phi = 0° plane. The figure provides essential insights into the antenna's main lobe characteristics, beamwidth, side lobe suppression, and overall radiation performance, which are crucial for high-frequency applications such as millimeter-wave (mmWave) communication, 5G, radar systems, and satellite links.

1. Main Lobe Characteristics

- The main lobe magnitude reaches a peak gain of 17 dB, indicating a highly directive radiation pattern.
- The main lobe direction is centered at 0°, which aligns with the intended beam orientation, confirming that the antenna efficiently radiates energy along the desired axis.
- The 3 dB beamwidth (angular width) is measured at 48.1°, which defines the region within which the antenna maintains at least half of its peak power. This balance between beamwidth and directivity suggests that the antenna can efficiently cover a moderate area while maintaining high gain.

2. Side Lobe Suppression

- The side lobe level (SLL) is -22 dB, which is significantly lower than the main lobe gain.
- This high level of side lobe suppression minimizes interference and reduces unwanted radiation, making the design suitable for applications where directional focus and low interference are critical, such as beamforming networks and high-resolution radar systems.
- The low side lobe level further enhances the antenna's ability to reject unwanted signals and improve signal-to-noise ratio (SNR) in communication systems.

3. Directionality and Beam Focusing

The symmetrical radiation pattern with a well-defined main lobe indicates highly directional behavior, which is beneficial for:

- **Point-to-point mmWave communication**: Directivity ensures efficient energy transfer with minimal losses.
- **Radar and sensing applications:** Narrow beamwidth provides precise target detection and tracking.
- **5G and beyond**: Supports spatial filtering, reducing interference from neighboring beams.

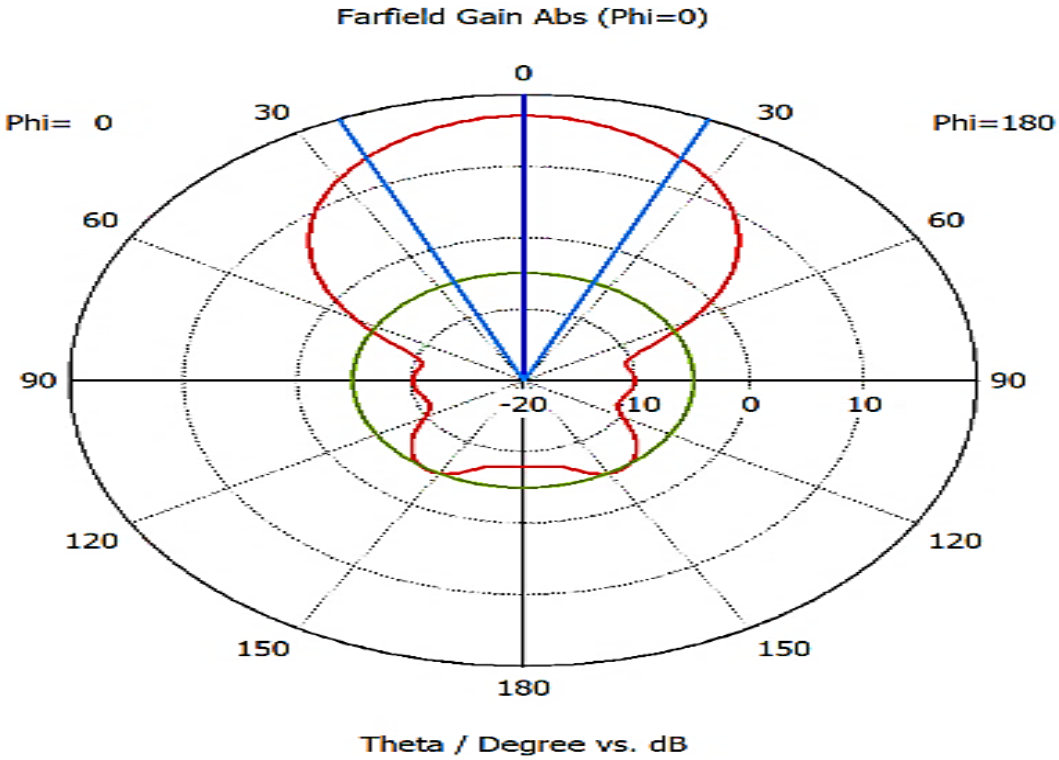

Fig. 11. E-Plane polar plot with HPBW = 48.1°

The polar plot in Fig.12 illustrates the far-field gain pattern of the antenna at 39.035 GHz for the Phi = 90° plane. This visualization provides critical insights into the antenna's directivity, beamwidth, and side lobe behavior, which are essential for understanding its suitability for high-frequency applications such as millimeter-wave (mmWave) communication, 5G networks, radar, and satellite systems.

1. Main Lobe Characteristics

- The peak gain of the main lobe is 17.2 dB, indicating strong directivity and efficient radiation performance at this frequency.
- The main lobe is centered at 1.0°, showing a slight deviation from 0°, which may result from minor phase variations in the antenna structure.
- The 3 dB beamwidth (angular width) is 9.7°, significantly narrower compared to the Phi = 0° plane. This suggests a more focused beam in this orientation, which is beneficial for applications requiring high precision and minimal signal dispersion.

2. Side Lobe and Radiation Efficiency

- The side lobe level (SLL) is -8.4 dB, meaning that the secondary lobes exhibit higher radiation compared to the Phi = 0° case.
- The presence of relatively higher side lobes may introduce interference, which should be considered for applications involving multi-antenna systems or beamforming.
- The increased side lobe radiation suggests some level of energy dispersion, which could be due to structural design, feed network imbalances, or material properties at this frequency.

3. Directionality and Beam Focusing

- The narrow beamwidth (9.7°**)** indicates highly focused radiation, making the antenna particularly suitable for point-to-point communication, radar tracking, and high-gain applications.
- The sharp and directive beam enhances spatial filtering capabilities, reducing the risk of interference from nearby sources in communication networks.

- The increased side lobe levels (-8.4 dB) suggest potential trade-offs between gain concentration and unwanted radiation, which may require further optimization depending on the use case.

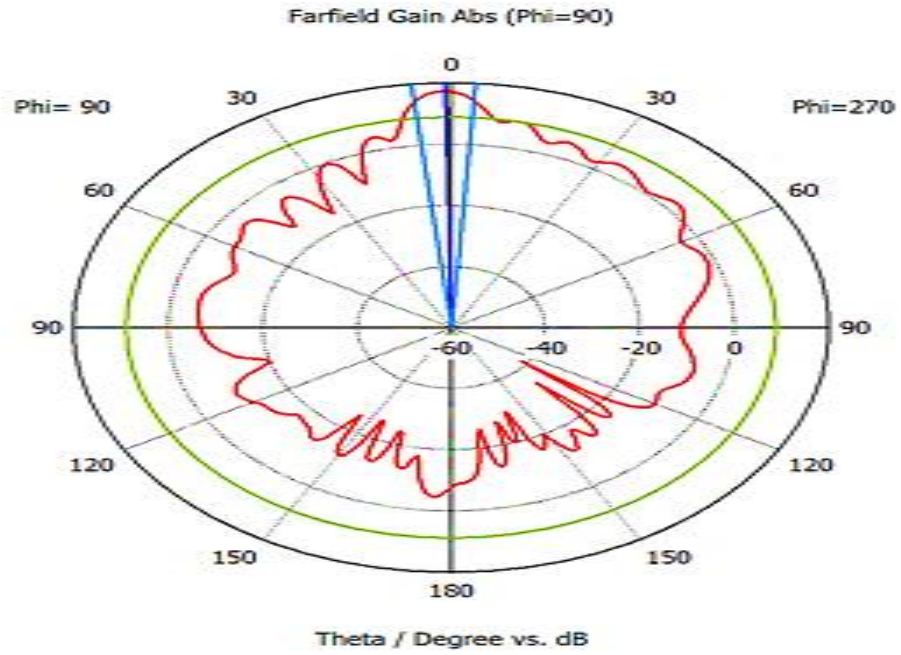

Fig. 12. H-Plane polar plot with HPBW = 9.7 °

Fig.13 presents the impedance (Z11) magnitude, and Fig.14 presents the impedance phase of a millimeter-wave (mmWave) antenna across a frequency range of 20 GHz to 65 GHz. A significant impedance value is observed at 39.035 GHz with a magnitude of 50.083 Ω and phase 0.068°, which is close to the standard 50 Ω, ensuring good impedance matching and efficient power transfer. The presence of peaks at various frequencies suggests the antenna's suitability for diverse mmWave applications, including 5G communications and high-frequency sensing. Proper impedance matching techniques may be required to optimize performance across the entire operational bandwidth.

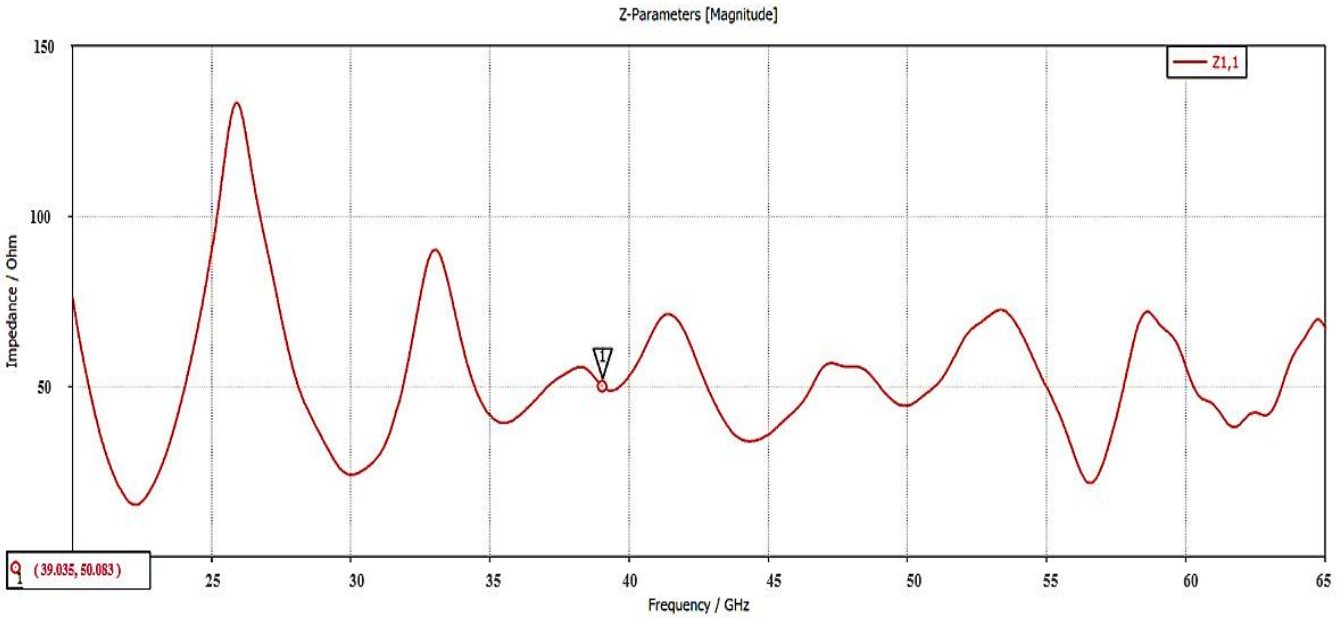

Fig. 13. The impedance magnitude (Z11) versus frequency

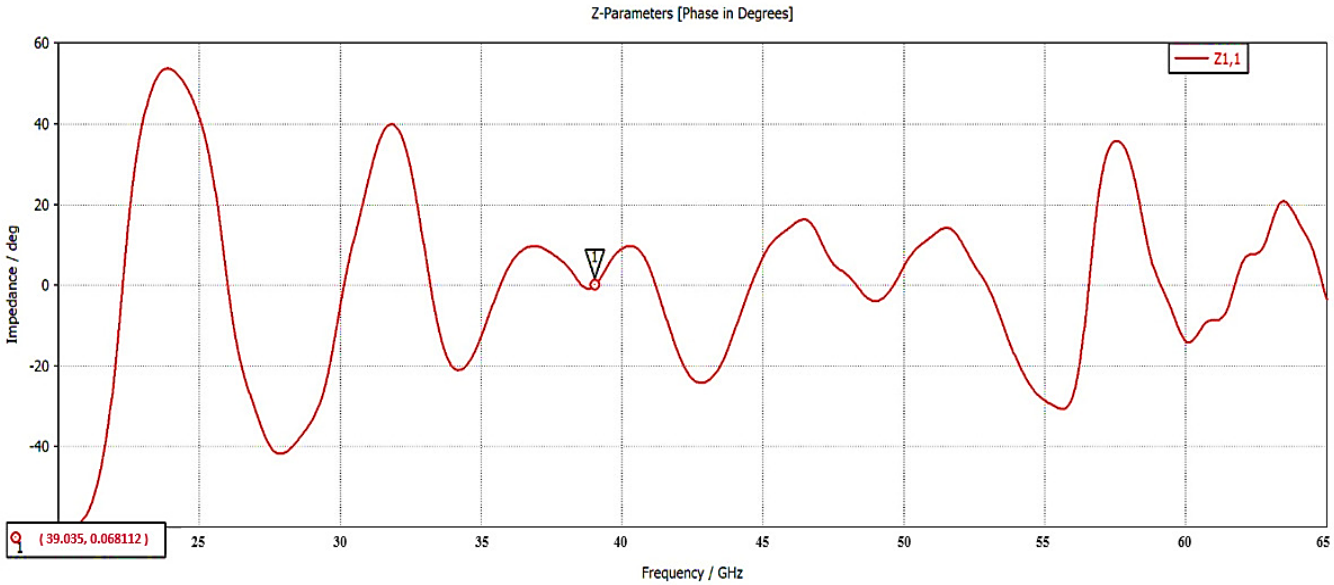

Fig. 14. The impedance (Z11) phase versus frequency.

Fig.15 illustrates the maximum 3D gain of a millimeter-wave (mmWave) antenna over a frequency range of 20 GHz to 50 GHz. The gain increases with frequency, reaching a peak value of 17.14 dB at 39.035 GHz, indicating optimal radiation performance at this frequency. Beyond this peak, the gain exhibits slight variations, suggesting stable performance across a broad bandwidth. The high gain values make the antenna well-suited for high-frequency applications such as 5G communications and radar systems, where directional radiation and efficiency are critical. Further optimization may be required to maintain consistent gain across the operational band.

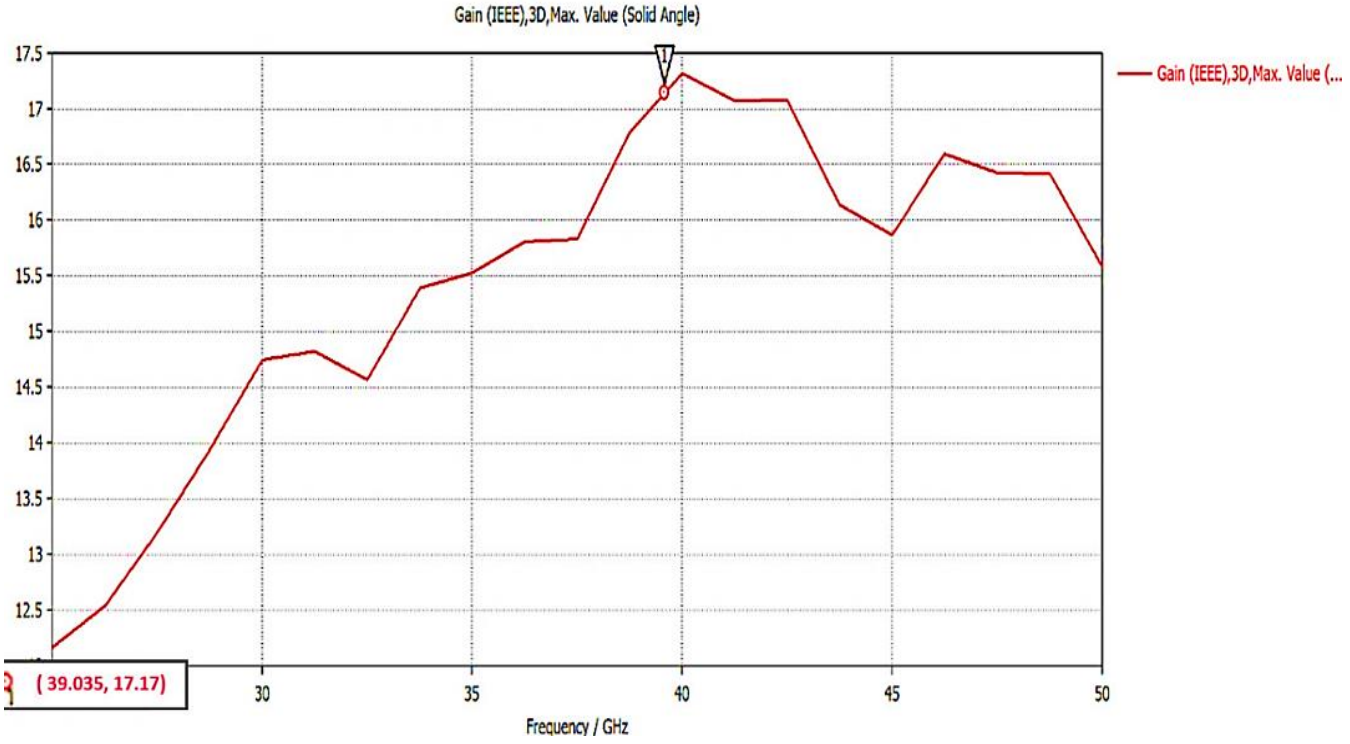

Fig. 15. The maximum 3D gain versus frequency

Fig. 16 indicates simulation results of current densities with the phase set to **0°**; it is clear from the presented figure that different current distributions have been obtained for each feeder. This surface current distribution plot at **39.035 GHz** reveals a well-defined and symmetrical pattern across the array elements, indicating consistent excitation and effective element placement. The peak surface current density reaches approximately **262.559 A/m²**, with values plotted on a logarithmic scale—ideal for capturing the dynamic range of current variation across the array. The regions of higher current intensity (red zones) suggest the active radiating elements or resonance points, while the lower intensity areas (blue tones) mark weaker current paths or possibly mutual coupling zones. The symmetry and distribution likely reflect good impedance matching and array design efficiency, especially with the phase set to **135°,** as indicated in Fig.17, which could hint at a specific beam-steering orientation or scanning direction.

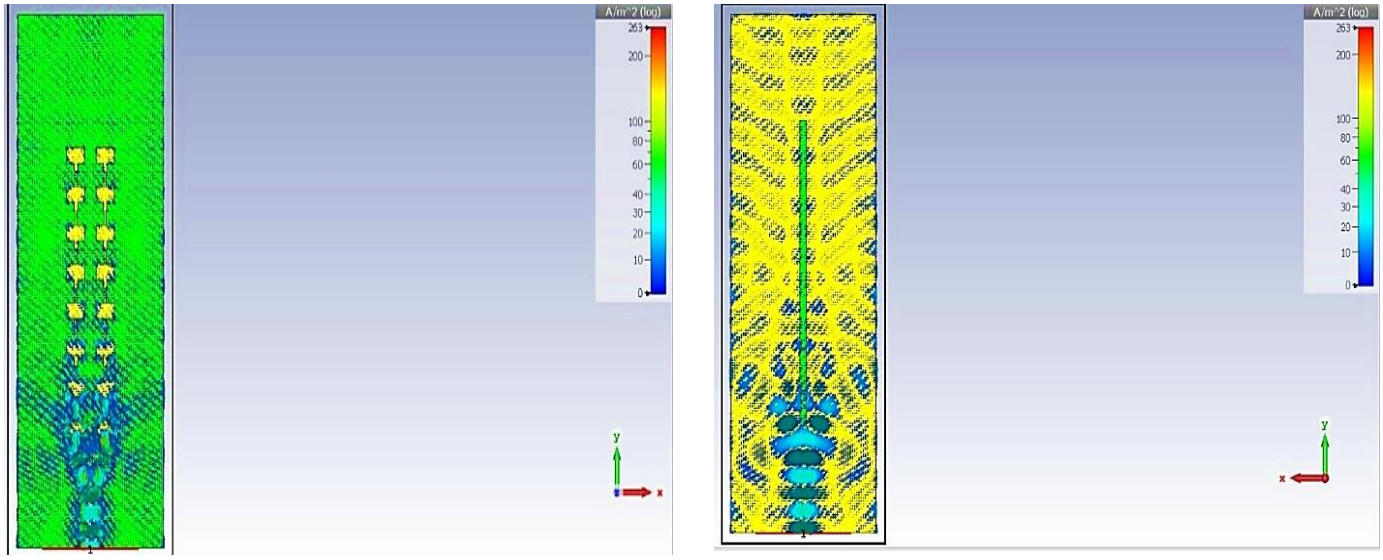

(a) (b)

Fig. 16. Surface current distribution with phase 0° (a) from array direction (b) from ground direction

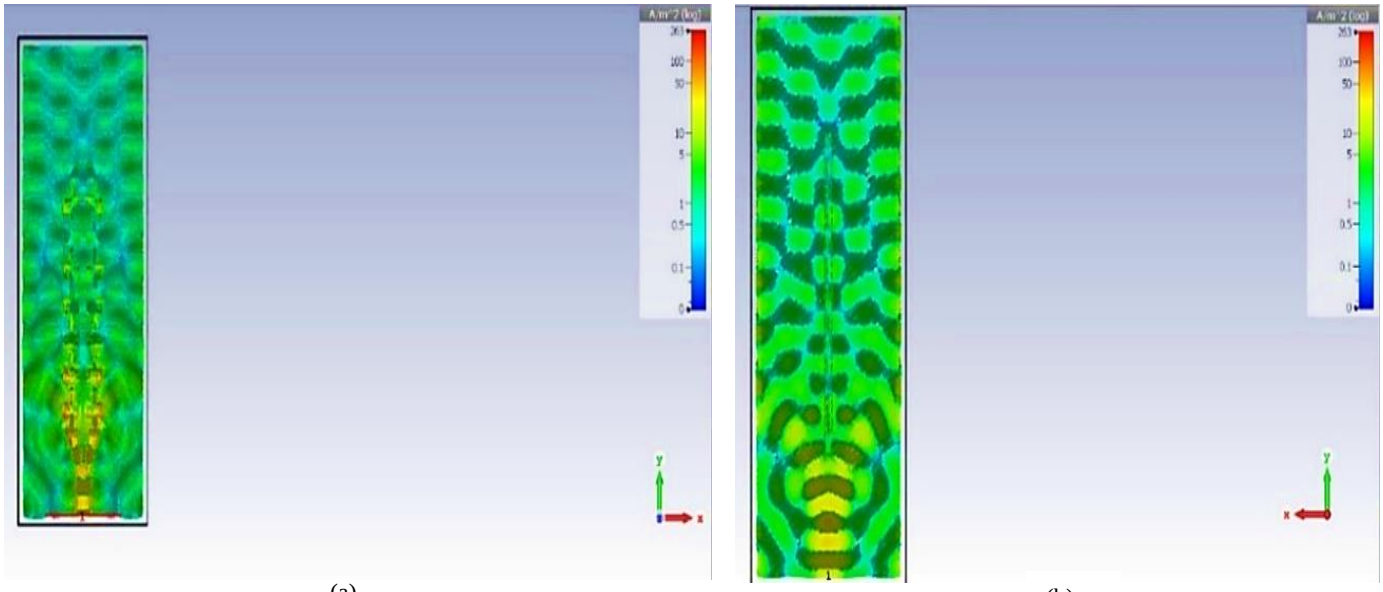

(a) (b)

Fig. 17. Surface current distribution with phase 135° (a) from array direction (b) from ground direction

VII. Parametric Study

To achieve stable and efficient impedance matching for the antenna array, a parametric study was conducted to evaluate the impact of substrate thickness (h) and feeding network dimensions on the antenna performance. Table III presents the influence of varying substrate thickness on key parameters, while Table IV examines the effect of feeder width (W_f) optimization for two selected feeder lengths: L_f = 6.76923 mm and L_f = 7.06923 mm. Based on this study, the optimal combination: h = 1.286 mm, L_f = 7.06923 mm**,** and W_f **=** 2.92 mm—was identified. This configuration achieves excellent impedance matching with S11 = -64.11 dB at the operating frequency of 39.035 GHz, alongside a bandwidth of 22.97 GHz**,** gain of 17.12 dB, and radiation efficiency of 90.8%**.** These results indicate a highly optimized design for high-frequency operation, balancing wide bandwidth and efficient radiation characteristics.

Table III
Parametric Study for Substrate Thickness (H) Effect on Antenna Parameters

h (mm)	Operating frequency (GHz)	S11 (dB)	Salability of simulation results of S11, VSWR and impedance
0.508	35.7	-37	High ripples in simulation results of S11, VSWR, and impedance
0.786	37.8	-53	Moderate ripples in simulation results of S11, VSWR, and impedance
1.286	39.035	-64.11	More Stable Simulation results of S11, VSWR, and impedance

Table IV
Parametric Study for Feeder Width On Antenna Parameters with H=1.286 mm

L_f (mm)	W_f (mm)	Operating frequency (GHz)	S11 (dB)
6.76923	1.92	38.45	-35.75
	2.42	38.675	-48.46
	2.92	39.08	-41.11
7.06923	1.92	39.36	-37.63
	2.42	39.585	-54.76
	2.92	39.035	-64.11

VIII. Conclusions

The proposed 39 GHz mmWave microstrip patch antenna exhibits excellent performance, positioning it as a strong candidate for next-generation 5G and high-frequency applications. Designed as a 16-element corporate-fed rectangular patch array on a Rogers RT5880 substrate, it achieves a wide operational bandwidth of **22.97 GHz** and a peak gain of **17.12 dB**. The incorporation of a Defected Ground Structure (DGS) significantly reduces mutual coupling and enhances both isolation and radiation efficiency, reaching **90.8%**. Outstanding impedance matching is demonstrated by a return loss of **–64.11 dB** at 39.035 GHz and a near-unity VSWR of **1.0012**, ensuring efficient power transfer and minimal reflection. Additionally, the antenna features a stable radiation pattern, low sidelobe levels, and consistent polarization, making it ideal for focused-beam applications including 5G mmWave communications, satellite links, radar systems, and hybrid optical–wireless networks. CST Microwave Studio simulations validate its superior performance over conventional designs, offering high efficiency, broad bandwidth, and strong directivity suitable for long-range, high-data-rate transmission. Future work will explore beamforming, MIMO integration, and adaptive frequency tuning, as well as flexible, dual-polarized, and multiband antenna designs. Additional efforts include optimizing performance in harsh environments and conducting experimental validation for real-world deployment.

References

[1] M. Nuriev, A. Kalyashina, Y. Smirnov, G. Gumerova, and G. Gadzhieva, "The 5G revolution transforming connectivity and powering innovations," *E3S Web Conf.*, vol. 515, p. 04008, 2024.

[2] M. J. Al-Dujaili and M. A. Al-dulaimi, "Fifth-generation telecommunications technologies: Features, architecture, challenges and solutions," *Wirel. Pers. Commun.*, vol. 128, no. 1, pp. 447–469, 2023.

[3] M. Agiwal, A. Roy, and N. Saxena, "Next generation 5G wireless networks: A comprehensive survey," *IEEE Commun. Surv. Tutor.*, vol. 18, no. 3, pp. 1617–1655, 2016.

[4] W. A. Ali, W. R. Anis, and H. A. Elshenawy, "Spectral efficiency enhancement in Massive MIMO system under pilot contamination," *Int. J. Commun. Syst.*, vol. 33, no. 8, p. e4342, 2020. [Online]. Available: https://doi.org/10.1002/dac.4342

[5] W. A. Ali, W. R. Anis, and H. A. Elshenawy, "Pilot contamination mitigation in Massive MIMO systems over Laplacian local scattering spatial correlation channels," in *Proc. 36th Nat. Radio Sci. Conf. (NRSC)*, Apr. 2019, pp. 153–162. [Online]. Available: https://doi.org/10.1109/NRSC.2019.8734639

[6] N. Al-Falahy and O. Y. Alani, "Millimetre wave frequency band as a candidate spectrum for 5G network architecture: A survey," *Phys. Commun.*, vol. 32, pp. 120–144, 2019.

[7] Y. Niu, Y. Li, D. Jin, L. Su, and A. V. Vasilakos, "A survey of millimeter wave communications (mmWave) for 5G: Opportunities and challenges," *Wirel. Netw.*, vol. 21, pp. 2657–2676, 2015.

[8] A. N. Uwaechia and N. M. Mahyuddin, "A comprehensive survey on millimeter wave communications for fifth-generation wireless networks: Feasibility and challenges," *IEEE Access*, vol. 8, pp. 62367–62414, 2020.

[9] M. K. Banafaa *et al.*, "A comprehensive survey on 5G-and-beyond networks with UAVs: Applications, emerging technologies, regulatory aspects, research trends and challenges," *IEEE Access*, vol. 12, pp. 7786–7826, 2024.

[10] M. D. Madhan and D. Subitha, "Millimeter-wave microstrip patch antenna design for 5G," *Int. J. Innov. Technol. Explor. Eng. (IJITEE)*, vol. 8, no. 12, pp. 1183–1187, 2019.

[11] G. Kim and S. Kim, "Design and analysis of dual polarized broadband microstrip patch antenna for 5G mmWave antenna module on FR4 substrate," IEEE Access, vol. 9, pp. 64306–64316, 2021.

[12] S. A. R. Parizi, "Bandwidth enhancement techniques," in *Microstrip Antennas: Trends in Research on*, vol. 1, 2017.

[13] D. G. Fang, C. Z. Luan, and Y. P. Xi, "Mutual coupling in microstrip antenna array: Evaluation, reduction, correction or compensation," in *Proc. IWAT*, Mar. 2005, pp. 37–40.

[14] B. A. Nel, A. K. Skrivervik, and M. Gustafsson, "Radiation Efficiency and Gain Bounds for Microstrip Patch Antennas," *arXiv preprint arXiv:2403.18844*, 2024.

[15] F. F. D. Araújo, A. L. P. D. S. Campos, R. V. D. A. Lira, A. Gomes, and A. G. d'Assunção, "Bandwidth enhancement of microstrip patch antenna using metasurface," *J. Microwaves Optoelectron. Electromagn. Appl.*, vol. 20, no. 1, pp. 105–117, 2021.

[16] R. Jedlicka, M. T. Poe, and K. Carver, "Measured mutual coupling between microstrip antennas," *IEEE Trans. Antennas Propag.*, vol. 29, no. 1, pp. 147–149, 1981.
[17] A. O. Watanabe, M. Ali, S. Y. B. Sayeed, R. R. Tummala, and M. R. Pulugurtha, "A review of 5G front-end systems package integration," *IEEE Trans. Compon. Packag. Manuf. Technol.*, vol. 11, no. 1, pp. 118–133, 2020.
[18] M. M. Zayed, M. Shokair, and S. Elagooz, "Underwater optical MIMO for high data-rate IoUT," *J. Opt.*, pp. 1–41, 2025. [Online]. Available: https://doi.org/10.1007/s12596-025-02493-1
[19] M. M. Zayed, S. Mohsen, A. Alghuried, H. Hijry, and M. Shokair, "IoUT-oriented an efficient CNN model for modulation schemes recognition in optical wireless communication systems," *IEEE Access*, 2024. [Online]. Available: https://doi.org/10.1109/ACCESS.2024.3515895
[20] W. A. Ali, M. H. Shaker, M. Shokair, and M. M. Zayed, "Green underwater communication for ROVs: Harnessing Li-Fi for sustainable and efficient marine operations," *J. Opt.*, pp. 1–27, 2025. [Online]. Available: https://doi.org/10.1007/s12596-025-02774-9
[21] M. M. Zayed, M. Shokair, S. Elagooz, and H. Elshenawy, "Multihop optical wireless underwater communication links utilizing various routing protocols for IoUT applications," *J. Opt.*, pp. 1–25, 2024. [Online]. Available: https://doi.org/10.1007/s12596-024-02290-2
[22] B. W. Aboshosha, M. M. Zayed, and R. A. Ramadan, "Enhancing Internet of Things security in healthcare using a blockchain-driven lightweight hashing system," *Beni-Suef Univ. J. Basic Appl. Sci.*, vol. 14, no. 1, pp. 1–30, 2025. [Online]. Available: https://doi.org/10.1186/s43088-025-00644-8
[23] N. Alaoui, R. I. Ben Melouka, M. R. Mekhatria, and I. Titouh, "High-performance 38 GHz millimeter wave antenna for 5G wireless application," *Int. J. Inf. Technol.*, pp. 1–8, 2025.
[24] J. Hatte, S. Mudda, K. M. Gayathri, and R. B. Patil, "Millimeter-wave dual-band (32/38 GHz) microstrip patch antenna for 5G communication," in *Proc. ICRIC*, vol. 2, pp. 225–237, 2022.
[25] I. Shaik and S. K. Veni, "Design and Analysis of a Compact 38 GHz Wideband Monopole Antenna for 5G mm-Wave Wireless Applications," *Prog. Electromagn. Res. C*, vol. 135, 2023.
[26] S. M. Shamim, U. S. Dina, N. Arafin, and S. Sultana, "Design of efficient 37 GHz millimeter wave microstrip patch antenna for 5G mobile application," *Plasmonics*, vol. 16, no. 4, pp. 1417–1425, 2021.
[27] S. H. Lee *et al.*, "Design and Performance Analysis of 5G Mobile Communication Array Antenna in Millimeter-Wave (mm-Wave) Band," *J. Korea Inst. Inf. Commun. Eng.*, vol. 24, no. 9, pp. 1165–1171, 2020.
[28] B. G. Hakanoğlu, B. Koç, H. Yalduz, Ş. E. Hayber, and M. Türkmen, "Comparative Analysis of the Effects of the Substrate Material and Deltoid Shaped Slots on Patch Antennas for 5G Networks at 37 GHz and 39 GHz," *Avrupa Bilim ve Teknol. Derg.*, pp. 405–411, 2020.
[29] S. I. Naqvi *et al.*, "An integrated antenna system for 4G and millimeter-wave 5G future handheld devices," *IEEE Access*, vol. 7, pp. 116555–116566, 2019.
[30] Y. Ghazaoui *et al.*, "Millimeter wave antenna with enhanced bandwidth for 5G wireless application," *J. Instrum.*, vol. 15, no. 01, p. T01003, 2020.
[31] S. Muhammad, I. Ya'u, A. S. Abubakar, and A. S. Yaro, "Design of single feed dual-band millimeter wave antenna for future 5G wireless applications," *Sci. World J.*, vol. 14, no. 1, pp. 84–87, 2019.
[32] M. A. Saada, T. Skaik, and R. Alhalabi, "Design of efficient microstrip linear antenna array for 5G communications systems," in *Proc. ICPET*, Oct. 2017, pp. 43–47.
[33] E. Sandi, A. D. Rusmono, A. Diamah, and K. Vinda, "Ultra-wideband Microstrip Array Antenna for 5G Millimeter-wave Applications," *J. Commun.*, vol. 15, no. 2, pp. 198–204, 2020.
[34] R. O. E. Mohamed, "Design of Efficient Millimeter Waves Planar Antennas For 5G Communication Systems," in *Proc. ICCCEEE*, Feb. 2021, pp. 1–6.
[35] A. S. Gaid, O. A. Qaid, and A. M. Alhakimi, "Microstrip antennas for next genertion wireless devices," in *Proc. ICOICE*, Dec. 2019, pp. 1–4.
[36] C. A. Balanis, *Antenna Theory: Analysis and Design*, 4th ed. Hoboken, NJ, USA: Wiley, 2015.
[37] I. J. Bahl, "A designer's guide to microstrip line," *Microwaves*, vol. 1, pp. 1–380, 1977.